Drug quantification in turbid media by fluorescence imaging combined with light-absorption correction using white Monte Carlo simulations

Haiyan Xie
Haichun Liu
Pontus Svenmarker
Johan Axelsson
Can T. Xu
Susanna Gräfe
Jesper Holm Lundeman
Haynes Pak Hay Cheng
Sune Svanberg
Niels Bendsoe
Peter E. Andersen
Katarina Svanberg
Stefan Andersson-Engels

Drug quantification in turbid media by fluorescence imaging combined with light-absorption correction using white Monte Carlo simulations

Haiyan Xie,[a] **Haichun Liu,**[a] **Pontus Svenmarker,**[a] **Johan Axelsson,**[a] **Can T. Xu,**[a] **Susanna Gräfe,**[b]
Jesper Holm Lundeman,[c] **Haynes Pak Hay Cheng,**[c] **Sune Svanberg,**[a] **Niels Bendsoe,**[d] **Peter E. Andersen,**[c]
Katarina Svanberg,[e] **and Stefan Andersson-Engels**[a]
[a]Lund University, Department of Physics, P.O. Box 118, SE-221 00, Lund, Sweden
[b]Biolitec AG, Research and Development, D-077 45, Jena, Germany
[c]Technical University of Denmark, DTU Fotonik, DK-4000, Roskilde, Denmark
[d]Lund University Hospital, Department of Dermatology and Venereology, SE-221 85, Lund, Sweden
[e]Lund University Hospital, Department of Oncology, SE-221 85, Lund, Sweden

Abstract. Accurate quantification of photosensitizers is in many cases a critical issue in photodynamic therapy. As a noninvasive and sensitive tool, fluorescence imaging has attracted particular interest for quantification in pre-clinical research. However, due to the absorption of excitation and emission light by turbid media, such as biological tissue, the detected fluorescence signal does not have a simple and unique dependence on the fluorophore concentration for different tissues, but depends in a complex way on other parameters as well. For this reason, little has been done on drug quantification *in vivo* by the fluorescence imaging technique. In this paper we present a novel approach to compensate for the light absorption in homogeneous turbid media both for the excitation and emission light, utilizing time-resolved fluorescence white Monte Carlo simulations combined with the Beer–Lambert law. This method shows that the corrected fluorescence intensity is almost proportional to the absolute fluorophore concentration. The results on controllable tissue phantoms and murine tissues are presented and show good correlations between the evaluated fluorescence intensities after the light-absorption correction and absolute fluorophore concentrations. These results suggest that the technique potentially provides the means to quantify the fluorophore concentration from fluorescence images. © *2011 Society of Photo-Optical Instrumentation Engineers (SPIE)*. [DOI: 10.1117/1.3585675]

1 Introduction

Photodynamic therapy (PDT) has been clinically accepted to treat certain types of malignant tumors as well as some non-malignant diseases.[1,2] In PDT a photosensitizer (PS) is administrated either systemically or topically. It is activated by irradiating appropriate light to the sensitized tumor. As the PS absorbs light, the gained energy can be transferred to nearby oxygen molecules, leading to the formation of highly reactive oxygen radicals and thereafter tissue damage. PDT is a nonthermal photochemical reaction, which requires the presence of a photosensitizing agent (i.e., PS), oxygen and light, simultaneously. In PDT, quantification of the PS in a noninvasive way is in many cases a critical issue, since light dosimetry, irradiation parameters, and therapeutic outcome depends significantly on the PS quantities distributed in the region of interest (ROI).

Various techniques have been proposed to quantify the PS concentration. In *ex vivo* animal experiments, high performance liquid chromatography (HPLC) of excised tissues is conventionally used as a gold standard for quantitative analysis of the PS concentration as well as for its pharmacokinetic behavior.[3] Optical techniques can offer alternatives and be used *in vivo*. Among

these techniques, absorption spectroscopy[4–7] provides a noninvasive tool for PS concentration studies. However, it suffers from a relatively poor detection sensitivity, limiting its applicability.[4] Most photosensitizing agents are, however, fluorescent, providing another possibility for measuring its concentration. Fluorescence has already been extensively used for tumor localization and to assess treatment progression during diagnostic screening or image-guided surgery to improve clinical decision-making and the therapeutic outcome (see e.g., Refs. 8–11).

Fluorescence spectroscopy (either in the point-monitoring or imaging mode) can also be used as a tool for PS concentration measurements.[4, 12–15] No tissue excision would be required in contrast to HPLC. Thus, it may constitute a tool for minimally invasive quantification studies providing *in vivo* capabilities. In these types of measurements, it is, however, a challenge to reduce the influence of the attenuation of the probing light. The signal depends not only on the concentration of the fluorophore but also on the optical properties, the detection geometry, and the tissue autofluorescence [i.e., the fluorescence from endogenous tissue fluorophores such as collagen or nicotinamide adenine dinucleotide (NADH)[16]], etc. Ultimately, these dependencies tend to decrease the correlation coefficient between the fluorescence signal and the true PS concentration.

Address all correspondence to: Haiyan Xie, Lund University, Department of Physics, P.O. Box 118, 22100 Lund, Sweden. Tel: 0046-46-222 3119; Fax: 0046-46-222 4250; E-mail: haiyan.xie@fysik.lth.se.

An alternative method would be to perform a tomographic reconstruction [fluorescence diffuse optical tomography-(FDOT)]. Such a procedure would obtain the fluorescence signal per unit volume tissue compensated for the light attenuation. The reconstruction is achieved by fitting the collected boundary fluence for multiple source-detector pairs to a forward propagation model, for example, the diffusion model. This somewhat limits the geometries possible in the measurements. Furthermore, FDOT suffers from the requirement of a sophisticated system, greatly increasing the system expense. Moreover, an increased computation time, usually unknown background, and that the reconstruction algorithm most often is very ill-conditioned makes the technique difficult to use in practice.[17–20] Image ratiometric quantification is therefore a commonly used method[12] to correct for these properties. Svensson et al. have suggested and shown that an image ratio of the fluorescence signal from the PS over tissue autofluorescence signal could provide a capability in real-time PS quantification in a defined murine organ.[21] However, different organs do not show the same dependence, probably due to their different optical properties. In Ref. 13, a double fluorescence/reflectance ratio was calculated for two different excitation sources. The excitation wavelengths were chosen to match the maximum and minimum of the fluorophore absorption spectrum. In this way, it was possible to compensate for the optical properties, and to obtain a signal that is only weakly dependent on these properties. This approach requires a sharp edge in the fluorophore absorption in order to facilitate a proper normalization. In Ref. 22, Themelis et al. employed a single fluorescence/remittance ratio approach to correct for the light attenuation effects. They managed to improve the correlation between the fluorescence intensity and fluorophore concentration approximately from 2.5:1 to 1.6:1 for the epi-illumination imaging and from 1.8:1 to 1.2:1 for the transillumination imaging at a five-fold absorption variation for the phantoms they constructed. None of these techniques compensates adequately for the absorption at both excitation and emission wavelengths. The ratio-based methods are thus generally limited to certain special cases.

In this paper we present a novel model-based light-absorption correction approach to obtain the fluorescence intensity originating from the fluorophores to accurately quantify the PS concentrations from the 2D fluorescence images. This method utilizes time-resolved fluorescence white Monte Carlo (FWMC) simulations in combination with the Beer–Lambert law for light absorption. It takes into account details of the light propagation in homogeneous turbid media and thus does not require separate multispectral fluorescence measurements. The results on tissue-like phantoms containing Rhodamine 6G and organs of mice following systemic administration of a liposomal formulation of meso-tetra hydroxyphenyl chlorin (m-THPC), are presented and show an almost linear response of the corrected fluorescence intensities to the chemically extracted fluorophore concentrations measured from HPLC, regardless of the tissue optical properties. The sensitivity of the results to the optical properties variation of the media in the model are also presented.

2 Materials and Methods

The light-absorption correction method based on 2D fluorescence images was first validated with a set of well controlled tissue-like phantoms containing the fluorescent dye Rhodamine 6G. Then the PS concentration was evaluated in excised murine tissues and compared to the results from the gold standard in terms of HPLC analysis of extracted tissue samples.

2.1 Phantom Preparation

Twenty homogeneous liquid tissue phantoms were prepared by mixing water (192.3 ml), Intralipid (Fresenius Kabi, Uppsala, Sweden; 200 mg/ml, 7.3 ml), India ink (Pelican Fount, Hannover, Germany; 1:100 stock solution prepared in our lab, 0 ml, 0.5 ml, 1.0 ml, 1.5 ml, respectively), and Rhodamine 6G, a fluorescent dye with similar emission spectra to fluorescent proteins (Lambda Physik, Göttingen, Germany; a concentration of 10 μm solution, 0.2 ml, 0.5 ml, 1.0 ml, 1.5 ml, 2.0 ml, respectively). The ranges of ink and dye concentrations were chosen to match the absorption and fluorescence for small animals for both the excitation and emission wavelengths.[23] Each phantom was placed in a cylindric glass container. The thickness of the phantom was 3.1 cm. The absorption and reduced scattering coefficient were measured with a time-of-flight (TOF) spectroscopy system, described in detail elsewhere.[24] The coefficients were measured at two wavelengths (632 and 660 nm). The absorption could be assumed constant over the wavelength range of interest, with the India ink as the absorber. For the reduced scattering, we assumed the relation

$$\mu_s'(\lambda) = a \cdot \lambda^{-b}, \tag{1}$$

where the parameters a and b were determined from the measurements. The anisotropy factor was assumed to be 0.87 at these two wavelengths.[25]

2.2 Photosensitizer

In the animal measurement, Fospeg® (Biolitec AG, Jena, Germany), a liposomal formulation of the active ingredient m-THPC, or temoporfin, was employed as the PS.[26,27] Liposomes are designed as carrier and delivery systems with the aim of improving the tumor accumulation behavior of the PS during PDT. The PS was diluted in 50 μl of 5% glucose. All compounds were stored at 4°C in the darkness. The extinction coefficients and fluorescence emission spectrum of m-THPC dissolved in ethanol were measured using a conventional spectrofluorometer (HORIBA Jobin Yvon GmbH, Unterhaching, Germany).

2.3 Animal Model

The study was performed on 30 female NMRI nu/nu mice (Harlan Winkelmann GmbH, Borchen, Germany). All animal experiments were carried out in compliance with the guidelines established by European Council Directive 86/909/EC and had been approved by the Thüringer Landesamt für Lebensmittelsicherheit und Verbraucherschutz, Weimar. A suspension of HT29 human colorectal carcinoma cells (0.1 ml of 8×10^7 cells/ml in 5% aqueous glucose solution) was inoculated subcutaneously 13 days before the measurements into the left and right hind thigh of six- to eight-week-old mice, weighing 22 to 25 g.

The optical properties for various murine tissues used in our data evaluation for some discrete wavelengths were obtained from Ref. 23. The reduced scattering coefficient was then extrapolated using Eq. (1). The absorption coefficient was

approximated in a similar way as a weighted sum of the concentrations of the blood (both oxy- and deoxy-hemoglobin) and water volume fractions in the organs, i.e.,

$$\mu_a(\lambda) = C_{\text{diff}}(\lambda, R_{\text{vessel}}) \cdot S_B \cdot [x\mu_{a_{\text{HbO}_2}}(\lambda)$$
$$+ (1 - x)\mu_{a_{\text{Hb}}}(\lambda)] + S_W \cdot \mu_{a_W}(\lambda), \qquad (2)$$

where $\mu_{a_{\text{HbO}_2}}(\lambda)$, $\mu_{a_{\text{Hb}}}(\lambda)$, and $\mu_{a_W}(\lambda)$ were the spectral absorption coefficients of oxy-haemoglobin (HbO$_2$), deoxy-haemoglobin (Hb) and water, respectively. $x = \text{HbO}_2/(\text{HbO}_2 + \text{Hb})$. S_B and S_W were blood and water volume fractions, respectively in the different mouse organs. The factor, $C_{\text{diff}}(\lambda, R_{\text{vessel}})$, was introduced to extend the applicability of the diffusion theory in homogeneous media to shorter wavelengths than 650 nm, due to the fact that blood is not a homogeneously distributed absorber but a strong absorber concentrated in the discrete blood vessels.[28] The mean vessel radius, R_{vessel}, was set to 60 μm.[29] Numerical values for all parameters in the model were selected as in Ref. [23]. Finally, the anisotropic factor was set to be 0.8 at both the excitation and emission wavelength.[30]

2.4 Animal Procedures

Fospeg® was injected into the tail vein of the mice 13 days after the tumor cell inoculation, when the tumors had reached a surface diameter of approximately 5 to 8 mm, and protruded approximately 2 to 3 mm above the skin surface. After injection of Fospeg®, the mice were kept in the dark and given food *ad libidum* until the experiment was performed. The animals were then sacrificed at different times (0.5, 2, 4, 8, and 18 h) after the PS injection. Blood was removed rapidly by cardiac puncture and organs (muscle, liver, kidney, and lung) were excised for fluorescence imaging measurements followed by HPLC analysis. Five mice without PS injection were used as controls.

2.5 HPLC Analysis

Immediately following the fluorescence imaging, the tissue samples were snap frozen and stored in the darkness until analyzed using chemical extraction and HPLC analysis. In preparation for the HPLC analysis, tissue samples were homogenized by cutting into small pieces, freeze dried for 24 h using a freeze dryer (Alpha 1-4 LSC, Martin Christ Gefriertrocknungsanlagen GmbH, Osterode am Harz, Germany), mixed with methanol and dimethyl sulfoxide (3:5, volume:volume), and continuously shaken for at least 12 h in a vortex mixer (Merck Eurolab, MELB 1719, Lutterworth, UK) operating at 2400 rpm. All samples were then spun at 16,000 rpm in a centrifuge (Microfuge, Heraeus, Germany) during 5 min. 1.0 ml of each supernatant was transferred to an HPLC vial. Details of the sample preparations and HPLC analysis are described in Refs. [21] and [31]. The results from the HPLC method of the excised tissue were used as gold standard for determining the drug concentrations. These values were correlated to the animal fluorescence measurements.

2.6 Fluorescence Imaging Measurements

Fluorescence images were acquired using the setup schematically depicted in Fig. 1. The excitation light was coupled into an
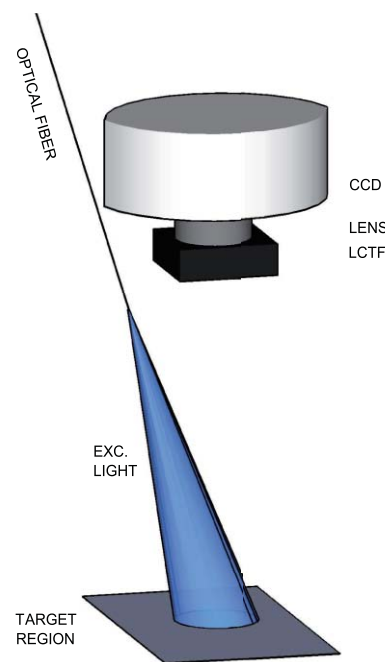

Fig. 1 Schematic picture showing the fluorescence imaging setup. The distal end of the fiber was positioned to obtain either a transillumination or an epi-fluorescence geometry.

optical fiber. The distal end of the fiber was positioned to obtain either a transillumination or an epi-fluorescence geometry.

For the phantom experiments, Rhodamine 6G was excited by an Nd:YAG laser (Viasho VA-I-N-532–200mW, Beijing, China) at 532 nm with a spot size of 3 mm in diameter from the bottom of the container. The fluorescence was spectrally filtered using a liquid crystal tunable filter (LCTF VIS 20-35, Varispec, CRI, Inc., Woburn, California). Images of transmitted fluorescence were acquired with the LCTF set to 600 nm, using a charge-coupled device (CCD) camera (Andor iXon DU-897, Belfast, Ireland) with a standard camera lens (50 mm focal length and f/1.8, Nikon, Tokyo, Japan). To suppress the transmitted laser light from reaching the camera, a long-pass, cut-off color-glass filter (OG-550, Schott Inc., W. Germany) was fixed between the sample and the LCTF.

For the animal measurement, a continuous-wave laser source at 405 nm developed at DTU Fotonik was used for excitation of the PS. It was based on a frequency doubled tapered diode amplifier placed in an external grating cavity with Littrow feedback, described in Ref. [32]. The entire laser system was built on a breadboard and placed on a mobile cart. The output power was 130 mW, out of which 70% was coupled into and delivered through an optical fiber mounted above the target. The spot size on the tissue was approximately 4 cm in diameter. The fluorescence images were captured by the CCD camera with the LCTF set to 652 nm (corresponding to m-THPC fluorescence peak) and 525 nm (tissue autofluorescence), respectively.

The fluorescence images were acquired in a dimmed room to avoid any artifacts from background light. Background images without the excitation light were also acquired using the same filter wavelength.
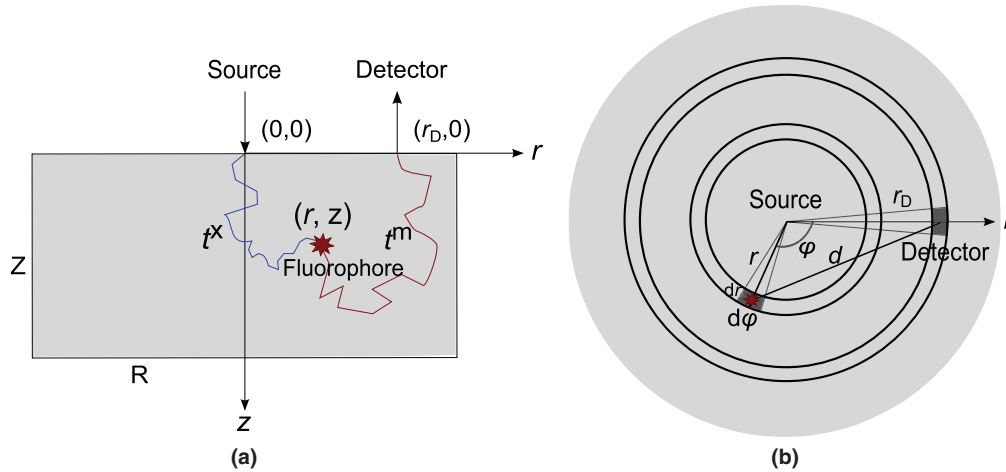
Fig. 2 Schematic diagram of the geometry used for fluorescence white Monte Carlo simulations. (a) The medium is divided into volume elements using small grids along the r and z axes. Similarly, time is divided into intervals with a size of dt. (b) View of the coordinate system used to calculate the convolution of excitation and emission light for a slab of thickness dz at z, where $d = (r^2 + r_D^2 + 2rr_D \cos \varphi)^{1/2}$.

2.7 Evaluation Procedure

The background image was subtracted pixel by pixel from each fluorescence image. The fluorescence intensity for an image was normalized with respect to the exposure time. Prior to the correction, all images obtained were cropped to the size of the ROI corresponding to the area where the fluorescence signal was measured for the phantom or the entire organ. Then the fluorescence intensity was computed as the average over each investigated sample.

2.7.1 Image ratio

The PS concentration within each animal organ was quantified by calculating a dimensionless contrast function resulting from forming a spectral ratio between the two detection bands:

$$R = F_{\text{image}}(652 \text{ nm})/F_{\text{image}}(525 \text{ nm}), \qquad (3)$$

where $F_{\text{image}}(652 \text{ nm})$ and $F_{\text{image}}(525 \text{ nm})$ denote the mean value of the fluorescence intensities within the ROI at the two wavelengths for each animal tissue sample.

2.7.2 Light absorption correction

For a series of nonabsorbing media with the same scattering coefficient and geometry but containing a different amount of fluorescence molecules (uniformly distributed), the fluorescence escaping from the surface is proportional to the concentration of the fluorophores. However, different media usually have different absorption coefficients, leading to different absorbed fractions both for the excitation and emission light. As a result, the fluorescence signal detected thus normally shows a strong dependence on the tissue type in addition to the fluorophore concentration. In principle, the absorptions of both the excitation and emission light can be compensated for by the Beer–Lambert law, if the temporal distribution of the escaping fluorescence is known. Thus, the linear dependence of the fluorescence intensity on fluorophore concentration could be reconstructed, independent on tissue type (or optical properties).

The temporal distribution of the fluorescence was simulated by a reverse-emission accelerated Monte Carlo (MC) approach,[33] which accelerated the fluorescence MC simulations considerably. To further save computation time, the method was modified and combined with the white Monte Carlo (WMC) simulation approach. The principle of WMC is explained in detail in Ref. 24. The WMC approach accelerates multispectral simulations as the solution for one set of optical properties (corresponding to one wavelength) can be rescaled to another set. This makes it only necessary to conduct one simulation run, independent of the number of wavelengths of interest. The simulation time can thus be greatly shortened, especially when modeling tissue fluorescence, where multiple wavelengths and different sets of optical properties are involved.

The medium simulated was assumed to be homogeneous and the fluorescent molecules to be uniformly distributed. The geometry used for the simulation is a cylinder with a radius of R and height of Z, as shown in Fig. 2. The optical properties of the medium at the excitation wavelength are described by the absorption coefficient μ_a^x, the scattering coefficient μ_s^x, and the anisotropy factor g^x. The corresponding parameters at the emission wavelength are μ_a^m, μ_s^m, and g^m, respectively. Furthermore, we define t^x as the time an excitation photon takes from the excitation light source to exciting a fluorophore, and t^m the time an emission photon takes from the fluorophore to the detector on the medium surface. For a nonabsorbing white medium with certain scattering coefficients μ_s^x and μ_s^m, the fluorescence intensities detected at a radial position r_D after time t^x and t^m are denoted as $F_W(r_D, t^x, t^m)$, the short term of $F_W(\mu_a^x = 0, \mu_a^m = 0, \mu_s^x, \mu_s^m, r_D, t^x, t^m)$. It could be simulated through a reverse-emission accelerated FWMC procedure, as defined in Ref. 33, by setting μ_a^x and μ_a^m to zero and convolving over space.

$$F_W(r_D, t^x, t^m) = \int_0^Z dz \int_0^R dr \int_0^{2\pi} d\varphi \, A_W\left(\mu_a^x = 0, \mu_s^x, r, z, t^x\right)$$

$$\times \phi_{\text{eff}}(r, \varphi, z) E_W\left(\mu_a^m = 0, \mu_s^m, d, z, t^m\right), \quad (4)$$

where $A_W(\mu_a^x = 0, \mu_s^x, r, z, t^x)$ is the probability per unit volume and unit time for an excitation photon to be absorbed at a fluorophore position (r, φ, z), after a time delay t^x from the injection point; $E_W(\mu_a^m = 0, \mu_s^m, d, z, t^m)$ is the probability

Table 1 Input parameters for white Monte Carlo simulations.

	No. photons	ϕ_{eff}	Grid resolution			Grid size			
			$dz\,(\mu m)$	$dr\,(\mu m)$	dt (ps)	nz	nr	nt_1	nt_2
Phantoms	2×10^6	0.25	500	500	10	61	120	400	400
Murine tissues	10^7	0.25	40	40	1	125	200	150	150

per unit volume and unit time to detect a fluorescence photon which originates from the fluorescence emission point which is located at a radial distance d and a depth z, after a delay t^m; $\phi_{\text{eff}}(r, \varphi, z)$ is the effective quantum yield, which is a constant in time and space and proportional to the fluorophore concentration. In our evaluation the decay of the fluorophore is assumed to be negligible. Values of input parameters used for the WMC simulations are stated in Table 1.

In the experiments, the excitation light was distributed over the medium surface. This effect was taken into account by

$$F_W^*(r_D, t^x, t^m) = F_W(r_D, t^x, t^m) \otimes S_{\text{Beam}}, \quad (5)$$

where $\otimes$ denotes the convolution, and S_{Beam} is the beam intensity profile on the medium surface.

If absorption is added to this white medium at both excitation and emission, the corresponding fluorescence intensities, $F_A^*(r_D, t^x, t^m)$, can be derived analytically from $F_W^*(r_D, t^x, t^m)$ using the Beer–Lambert law:

$$F_A^*(r_D, t^x, t^m) = F_W^*(r_D, t^x, t^m) \exp\left[-\mu_a^x v t^x\right] \exp\left[-\mu_a^m v t^m\right], \quad (6)$$

where $v = c/n$ is the light speed in the medium with a refractive index n. Integrating over the time, we will get a signal corresponding to the recorded fluorescence signal from a pixel at a radius r_D, or a Cartesian position (x, y) in the image, where $r_D = (x^2 + y^2)^{1/2}$. We denote this $F_{\text{image}}(x, y)$:

$$F_{\text{image}}(x, y) = F_{\text{image}}(r_D) = \int_{t^x} \int_{t^m} F_A^*(r_D, t^x, t^m) dt^x dt^m. \quad (7)$$

Then the total intensity from the image can be obtained by summing up all over the pixels:

$$F_{\text{image}} = \sum_{x,y} F_{\text{image}}(x, y). \quad (8)$$

By defining a calculated correction factor

$$\Delta \equiv \frac{\int_{t^x} \int_{t^m} \oint_{\text{ROI}} F_W^*(r_D, t^x, t^m) dt^x dt^m ds}{F_{\text{image}}}, \quad (9)$$

where s denotes the surface integral, and ROI is the evaluated region of interest from which the fluorescence is measured, we get

$$F_{\text{image}} \cdot \Delta \propto \int_{t^x} \int_{t^m} \oint_{\text{ROI}} F_W^*(r_D, t^x, t^m) dt^x dt^m ds \propto \phi_{\text{eff}} \propto \text{Conc}, \quad (10)$$

where Conc is the fluorophore concentration to be determined. This indicates the corrected fluorescence intensity, $F_{\text{image}} \cdot \Delta$, will be proportional to the fluorophore concentration.

3 Results

3.1 Time-Resolved Fluorescence Distribution from the FWMC Simulations

The simulated temporal distribution of the fluorescence signal $F(r_D, t^x, t^m, z_D)$ is plotted in Fig. 3. This corresponds to the detected signal at a surface of the simulated phantom at a radial distance $r_D = 5.0$ mm, where z_D indicates if the detector is at the bottom (the left column, $z_D = 3.1$ cm, corresponding to the transillumination geometry) or the top surface (the right column,
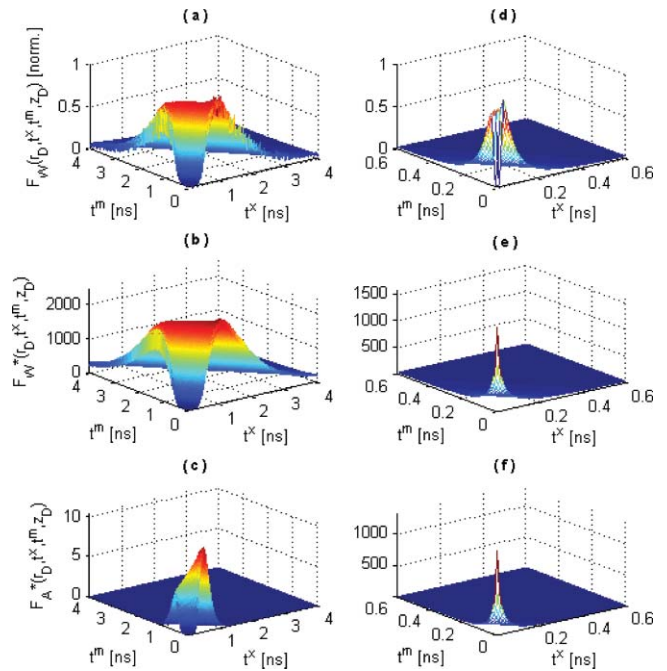

Fig. 3 Simulated temporal distribution of the fluorescence for the phantom at $r_D = 5.0$ mm. The left column illustrates the fluorescence at $Z_D = 3.1$ cm, i.e., for the transillumination geometry. The fluorescence intensity has been normalized to its peak signal. The right column shows the corresponding data at $Z_D = 0$, i.e., for the epi-fluorescence geometry. The top row show the results for a white medium when all the incident photons were injected at the origin; in (b) and (e) a uniform flat beam was incident all over the surface of this white medium; while in (c) and (f) an absorption of $\mu_a^x = \mu_a^m = 0.37$ cm^{-1} is added. In the simulations, reduced scattering coefficients of $\mu_s'^x = 10.07$ cm^{-1} and $\mu_s'^m = 8.30$ cm^{-1} were used. Values of the other parameters are listed in Table 1.
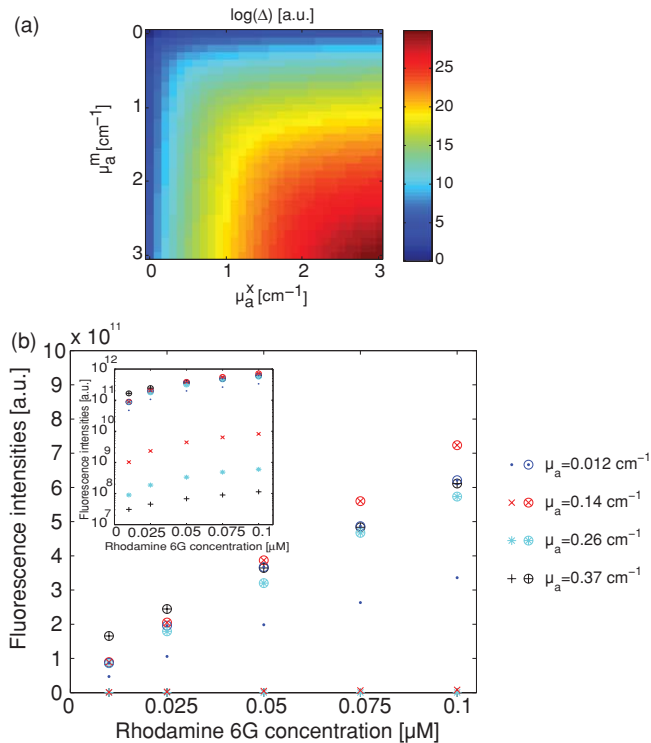
(a)

(b)

Fig. 4 (a) Dependence of the correction factor on phantom absorption coefficients for the transillumination geometry. (b) Scatter plots showing the fluorescence signals captured at 600 nm before (markers without circles) and after (with circles) the light-absorption correction versus the true dye concentrations for liquid tissue-like phantoms, where the absorption coefficients are the same at the 532-nm excitation and 600-nm emission, i.e., $\mu_a = \mu_a^x = \mu_a^m$. The inset shows the same data in the semi-log scale.

$z_D = 0$ cm, the epi-fluorescence geometry). The subplots in the top row show the results for a point source at the top center of a white medium, i.e., with zero-absorption. It can be seen that most of the excitation light has a large probability to be absorbed and the fluorescence reaches the detector within a much longer time in the transillumination geometry [Fig. 3(a)] than in the epi-fluorescence geometry [Fig. 3(d)]. For a flat light source with uniform power distribution irradiating all over the surface of the white medium, the fluorescence signal in the point source case was convolved with the beam intensity profile on the total surface. The result of that is shown in the middle row. The signal is increased by a factor of approximately one thousand. When a certain absorption was added to the white medium, Eq. (6) was applied to calculate the absorbed light. The results are illustrated in the bottom row. Photons with a long traveling time are absorbed, resulting in a decreased fluorescence signal.

For the phantom, the total simulation time is approximately 3 h for one single FWMC process, running on a Intel Duo Core 2-GHz processor. For the smaller grids corresponding to the animal case, the simulation time is approximately 10 h.

3.2 *Phantom Measurements*

Our light-absorption correction method was first tested on homogeneous well-controlled tissue-like phantoms. From the TOF measurement, the absorption coefficients of the phantoms with
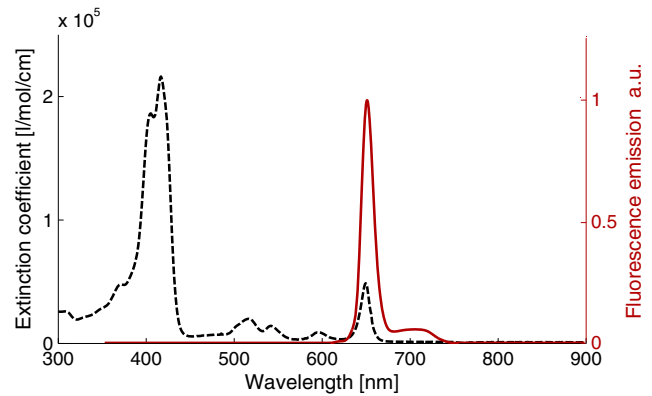

Fig. 5 The extinction coefficients (dashed line) and the fluorescence emission spectrum (solid line) of m-THPC when excited at 405 nm in ethanol.

the same ink concentration were the same at both 532 and 600 nm, as the India ink absorption is very flat over this wavelength range. For different ink concentrations, the results were 0.37, 0.26, 0.14, and 0.012 cm^{-1}, respectively. The reduced scattering coefficients were measured and extrapolated to be 10.10 cm^{-1} at 532 nm and 8.30 cm^{-1} at 600 nm.

The simulated dependence of the correction factor on different absorption coefficients at the excitation and emission wavelength is shown in Fig. 4(a). For the four sets of phantoms with different absorptions, the correction factor was $\Delta = 5303$, 949, 87, and 2, respectively. The large variation in Δ illustrates that the fluorescence signal from the surface is heavily dependent on the optical properties of the absorbing medium. Figure 4(b) shows the correlation between the fluorescence signal and the fluorescent dye (Rhodamine 6G) concentrations before and after the light-absorption correction, respectively. The markers without circles represent the raw signals directly from the images, while the markers with circles representing the corrected fluorescence intensities, which were achieved by multiplying the measured fluorescence from the images by the corresponding simulated Δ. The correlation between the fluorescence signal and the fluorophore concentration is dramatically improved from 3000:1 to 1.3:1.

3.3 *Animal Measurements*

The extinction coefficients and fluorescence emission spectrum of m-THPC dissolved in ethanol are plotted in Fig. 5, which shows a high extinction coefficient at 405 nm and strong fluorescent emission at 652 nm.

For the animal measurements, the data from the HPLC method were regarded as the absolute PS concentrations. Figure 6 shows some fluorescence images of the murine organs *ex vivo*, acquired from the imaging setup. Both the image spectral ratio [$F_{image}(652\ nm)/F_{image}(525\ nm)$] and light-absorption correction method [$F_{image}(652\ nm) \cdot \Delta$] were evaluated for the different types of murine organs. The results are shown in Figs. 7 and 8. The subplots on the left of Figs. 7 and 8 show the correlations between the raw fluorescence signals at 652 nm directly from the images and the PS concentrations. The slope of the linear fit varies from 5900 for muscle to 720 for lung (8.3:1). That is to say, no universal correlation curve could adequately fit
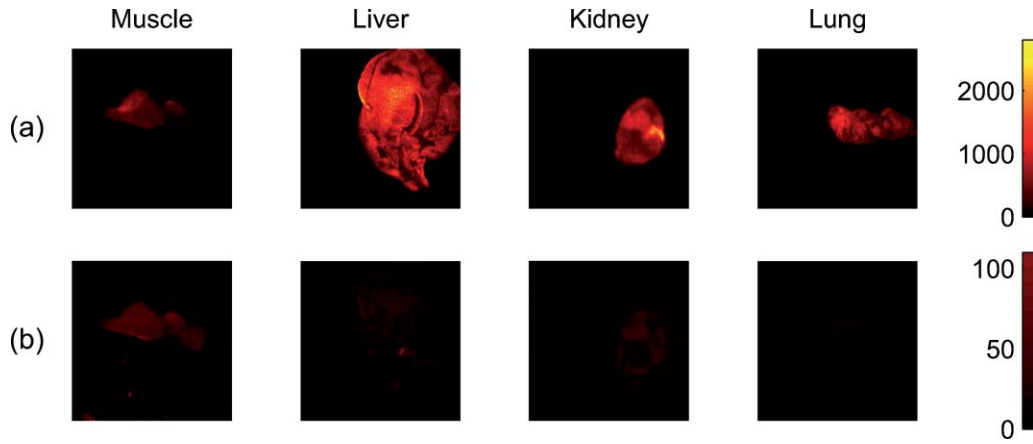
Fig. 6 Fluorescence images of some animal organs *ex vivo* captured at different emission wavelengths with an exposure time of 11 s. The color bars indicate fluorescence intensity after background subtraction. (a) The top row shows the images taken with the LCTF set to 652 nm (corresponding to the maximal drug fluorescence), while (b) the bottom row shows the images at 525 nm (tissue autofluorescence).
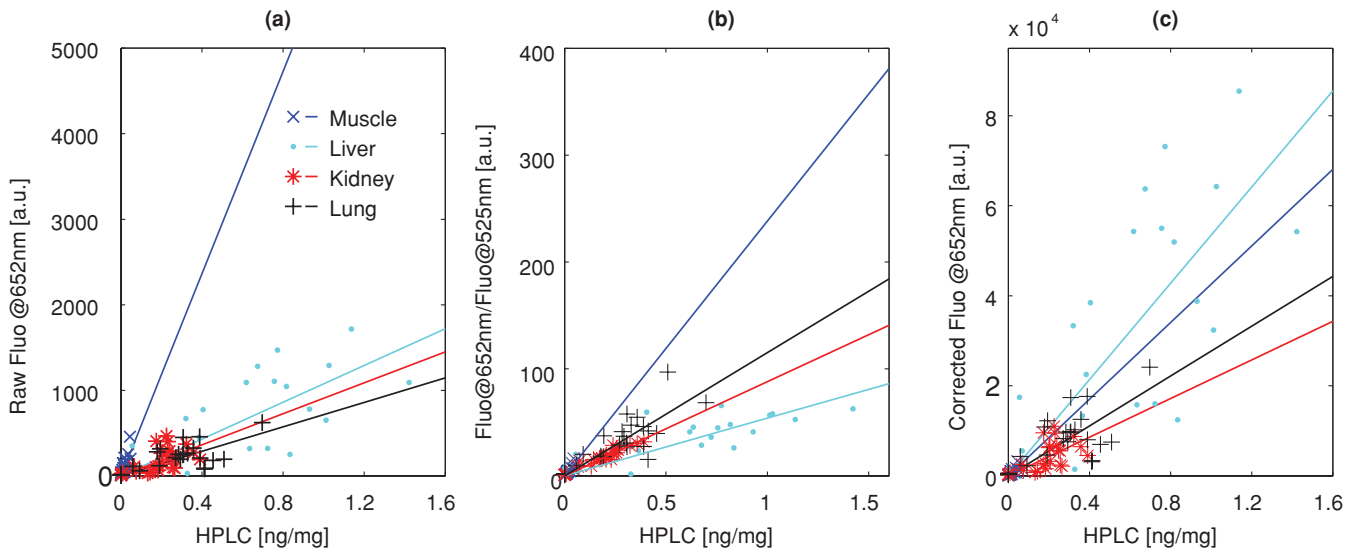

Fig. 7 Scatter plots showing (a) the fluorescence signals captured at 652 nm versus the HPLC values for individual organs, where a linear fit of the data points for each type of organs (solid line) is also shown; (b) the spectral ratio of the fluorescence intensities at 652 nm to that at 525 nm; and (c) the fluorescence signals after the light-absorption correction versus the HPLC values.
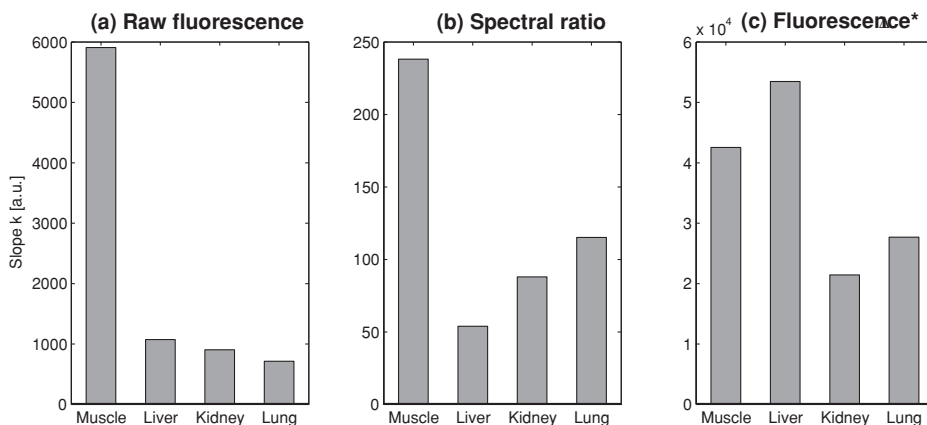

Fig. 8 Comparison of the linear fit slopes between the fluorescence signals and the HPLC values. The methods are the same as stated in Fig. 7.

Table 2 Optical properties of different organs.

Organs	μ_a^x(cm^{-1})	μ_a^m(cm^{-1})	μ_s^x(cm^{-1})	μ_s^m(cm^{-1})	$g^x = g^m(-)$
Muscle	6.2	0.4	88.7	23.0	0.8
Liver	26.5	1.8	57.5	34.9	0.8
Kidney	4.9	0.3	240.9	117.4	0.8
Lung	13.5	0.6	142.0	110.0	0.8

the fluorescence imaging data and the HPLC values, mainly due to the varying optical properties of the tissue under investigation. As shown in the middle columns, the slope from the spectral ratio varies from 240 for muscle to 60 for liver (4.4:1). After the absorbed light is compensated for, using the optical properties of a different type of murine organs listed in Table 2, the result on the right shows the slope varying from 53,500 for liver to 21,400 for lung (2.5:1).

4 Discussion

The simulated time-resolved fluorescence signal provides us with a clear picture of how the excitation and emitted photons migrate in the medium. With the information of the photomigration time, one can simulate the amount of light which is absorbed within the turbid medium, using the proposed absorption correction method. As demonstrated with tissue-like phantoms in Fig. 4(b), the correlation between the corrected (intrinsic) fluorescence signal and the dye concentration has been dramatically improved by approximately 2000-fold in comparison to the uncorrected signal, when absorption of the phantoms was varied over a wide range (approximately by a factor of 30). However, the corrected correlation is not a perfect single line (about 30% error in the correlation) for different sets of optical properties. This results mainly from about a 10% relative error in the optical properties measured by the TOF spectroscopy system.[34] Therefore, we tested the sensitivity of Δ due to the error in the measured optical properties by altering them to a ±10% variation, while the other parameters remained the same in the simulations. How Δ is affected for the set of phantoms with the highest absorption and scattering coefficients ($\mu_a^x = \mu_a^m = 0.37$ cm^{-1}, $\mu_s'^x = 10.10$ cm^{-1}, $\mu_s'^m = 8.30$ cm^{-1}) is shown in Tables 3 and 4, respectively. The relative change in Δ is within the range of -18% to $+36\%$. For the other phantoms, a smaller variation in Δ was obtained for lower values of the optical properties. Provided more accurate optical properties, one could expect a better correlation between the fluorescence and fluorophore concentrations. In addition, photobleaching of Rhodamine 6G (which also could provide an error) is not relevant due to the low light fluence and short acquisition time used.

For the animal study, Fospeg® content *ex vivo* in murine organs was quantified. This drug contains the active ingredient m-THPC, and therefore is interesting as a PDT sensitizer. The observed signal level directly from the fluorescence imaging measurement is affected by many factors. It generally leads to a poor correlation between the signal level and drug concentration, as shown in Figs. 7(a) and 8(a). The fitted linear slope of the raw fluorescence signals at 652 nm varies drastically between different organs. The large variations in the raw signals indicate that absorption caused by tissue should be taken into account to allow quantification of the PS in the tissue samples. Tissue absorption at the interesting wavelengths is mostly dependent on the amount of hemoglobin (both oxy- and deoxy-hemoglobin) in the tissue. The high absorbance in lung, kidney, and liver is caused by high blood contents, attenuating both the excitation and emission light. This effect explains the lower slope of the correlation curves for these organs as compared to those for muscle and skin. The detailed selectivity and biodistribution of Fospeg® following systemic administration were studied separately in Ref. 31.

To compensate for the tissue absorbed light, the optical properties for different murine organs need to be known. Values from literatures vary a lot and seem not fully consistent between tissue types. The large variation in literature values results from the fact that measurements were performed on tissues from different species, *in vitro* or *in vivo*, and at a great variety of sample preparation techniques and other experimental conditions. In the preparation period of the tissue samples in this study, bleeding during organ removal caused partial loss of the blood resulting in a variation of absorption coefficient even for the same type of tissues. As mentioned above, we do not have the precise values of the tissue optical properties. Instead, the tabulated values from Ref. 23 were used. They could only be interpreted as reasonable but rough estimates of the true mouse tissue optical properties. This is one of the main reasons why the correlation is not as good as that for the phantom. The sensitivity of the correction factor to tissue absorption coefficients are also examined for the liver with highest absorption ($\mu_a^x = 26.5$ cm^{-1}, $\mu_a^m = 1.8$ cm^{-1}, $\mu_s'^x = 11.5$ cm^{-1}, $\mu_s'^m = 7.0$ cm^{-1}). In Table 5, the absorption coefficients have been altered by ±30%, resulting in a variation in Δ from -34% to $+41\%$. Apparently this variation is less sensitive than that of the phantoms due to the much shorter migration pathlengths the photons spend in the epi-fluorescence geometry. Furthermore, if the tissue optical properties could be measured individually for each tissue investigated, simultaneously with the fluorescence imaging measurements, the correlation could be further improved.

The absorption correction method proposed in this study is based on assumptions that the fluorescent drug is homogeneously distributed within these tissues, and that all tissues have homogeneous optical properties. Unfortunately very little is known about distribution of this new drug following system-

Table 3 Sensitivity of the simulated correction factor to absorption coefficients of the phantoms.

	(μ_a^x, μ_a^m)	$(\mu_a^x - 10\%, \mu_a^m)$	$(\mu_a^x + 10\%, \mu_a^m)$	$(\mu_a^x, \mu_a^m - 10\%)$	$(\mu_a^x, \mu_a^m + 10\%)$
Variation in Δ	0	-23%	$+26\%$	-27%	$+32\%$

Table 4 Sensitivity of the simulated correction factor to scattering coefficients of the phantoms.

	$(\mu_s'^x, \mu_s'^m)$	$(\mu_s'^x - 10\%, \mu_s'^m)$	$(\mu_s'^x + 10\%, \mu_s'^m)$	$(\mu_s'^x, \mu_s'^m - 10\%)$	$(\mu_s'^x, \mu_s'^m + 10\%)$
Variation in Δ	0	-22%	$+25\%$	-18%	$+19\%$

atic administration. Nonetheless, we believe it is reasonable to assume a homogeneous fluorophore distribution. The assumptions are based on the following considerations and facts. First, the drug was systemically administrated to the animals. This suggests, in a first order approximation, a relatively homogeneous distribution in the tissues. Second, the time delays between drug injection and the measurements are relatively long in this study, again suggesting a relatively homogenous distribution. In addition, the tumors in this study are relatively small without visible necrotic regions that would cause an inhomogenous distribution. Actually, the inhomogeneity of the fluorescence can somehow be examined from the spatial distribution of the fluorescence ratio analyzed. From the fluorescence ratio image, a rather homogeneously fluorescence is present across the organ surface. Any spatial variation in raw data images for a single wavelength is mostly due to nonuniform illumination, variations in the distance, and the angle between the tissue surface and light source. In this study the fluorescence measurements are correlated with absolute drug concentration using chemical extraction and HPLC analysis, where the tissues were homogenized in preparation and the results were considered as a gold standard. This technique also relies on a homogeneous distribution.

It is known that the fluorescence intensity sometimes exhibits local variations in certain tissue structures due to light reabsorption or fluctuations in fluorescence yield due to the local fluorophore environment. The intra-animal variation in mTHPC concentration has been investigated by Kruijt et al. They investigated intratumoral localization of Foslip® (a different liposomal formulation of mTHPC in rat liver).[35] For short drug-light intervals, the drug is vascularly targeted, whereas longer time periods (>3 h) enable the PS to diffuse into the nearby tissues.[3] They found an overall homogeneous distribution of mTHPC on the macroscopic scale, while it was heterogeneous on a submillimeter spatial scale. The macroscopic fluorescence imaging setup and chemical extraction do not have the spatial resolution to pick up such a small spatial heterogeneity. Instead these techniques averaged the fluorescence intensities and homogenized the tissues in the chemical extraction. In fact, the absorption coefficient of animal tissues at 405-nm excitation wavelength is on the order of tens of cm^{-1}. When the fluorescence is excited at 405 nm, the effective penetration depth into tissue is typically on the order of hundreds of micrometers. In practice we are sampling a relatively small volume of tissues. This might also

decrease the correlation between the fluorescence signal and PS concentration.

Tissue autofluorescence could be another issue to slightly influence the measured fluorescence intensities and thus the resulting correlation. When excited by UV- or blue radiation, tissue autofluorescence has a broad spectrum without any distinct spectral features and slightly overlaps the drug fluorescence signals. The cross-talk will give a background in the detection. Johansson et al.,[4] and Svensson et al.[21] discussed how the influence of this cross-talk can be minimized for fluorophore assessments. In this work, another approach to handle the tissue autofluorescence was employed, using a dimensionless contrast function, namely the fluorescence ratio between the m-THPC emission peak at 652 nm and the strongest tissue autofluorescence at 525 nm, to study the drug concentrations. This approach improves the correlation between the fluorescence signals and the absolute drug content, yet not good enough, as shown in Figs. 7(b) and 8(b). To reduce the tissue autofluorescence, fluorescence imaging in the near-infrared was utilized in Ref. 22, since autofluorescence is much smaller than in the visible. Furthermore, a halogen lamp for white-light color imaging was employed to get the attenuation image, which had to be selected where the fluorophore of interest does not fluoresce. Therefore, the ratio-based quantification method has a quite strict limit on the spectral bands. It can not be applied in general cases. A significant advantage of the now proposed light-absorption correction method is that it does not have strict requirements on the spectral bands as in the ratiometric quantification methods.

Photodegradation of Temoporfin over time is usually expected in the fluorescence measurement, in particular in relation to the ultimate goal of using this technique for quantification of PS concentration during PDT. Normally photobleaching depends much on irradiance. Bendsoe et al. reported a photobleaching of about 30% to 35% after 200 s in a liposome formulation based on dipalmitoylphosphatidylcholine of m-THPC, with an irradiation of 20 J/cm^2 at 652-nm excitation.[36] In comparison, the fluence rate is 7 mW/cm^2 at 405-nm excitation in our measurement, which should translate in that the photodegradation is negligible within the imaging acquisition time (11 s). Based on this point, the light-induced changes in the resulting absolute PS concentration, which was obtained from HPLC analysis after fluorescence measurement, is also at an acceptable

Table 5 Sensitivity of the simulated correction factor to absorption coefficients of murine livers.

	(μ_a^x, μ_a^m)	$(\mu_a^x - 30\%, \mu_a^m)$	$(\mu_a^x + 30\%, \mu_a^m)$	$(\mu_a^x, \mu_a^m - 30\%)$	$(\mu_a^x, \mu_a^m + 30\%)$
Variation in Δ	0	-34%	$+41\%$	-10%	$+9\%$

level. It is worthwhile to point out that the fluorophore lifetime does not influence the correlation in the model at all, since the absorbed light depends only on the photon migration time.

5 Conclusion

In conclusion, this paper has shown that the fluorescence imaging technique can be used as a noninvasive and sensitive tool to quantify the fluorescent markers in homogeneous turbid media, using the novel light-absorption correction approach combining the fluorescence imaging and FWMC simulations. The results on both the well-controlled tissue-like phantoms and *ex vivo* animal tissues have shown that this method provides an acceptable quantification of fluorescent molecule markers in media with known geometry and optical properties at both the excitation and emission wavelengths. An improved linear correlation with the true concentrations is obtained independent of the tissue optical properties, since this method efficiently compensates for light attenuation and thus more directly relates to the intrinsic fluorescence signal levels from the fluorophores. This approach offers the advantages of minimizing the dependence on the tissue optical properties, a very low concentration detection limit, and wide spectral bands. The sensitivity of the results to the medium optical properties variation are presented and discussed, in order to point toward the possible future improvement of this technique.

In future work, it is highly desirable to combine the sensitivity of the fluorescence imaging technique with the tissue optical properties measurements to constitute an even better and more reliable fluorophore concentration estimate. The absorption correction and image ratio methods could also be combined to compensate for tissue autofluorescence.

1. A. Johansson and S. Andersson-Engels, Chapter 8 in *Laser Imaging and Manipulation in Cell Biology*, pp. 167–199, Wiley-VCH, Verlag (2010).
2. K. Svanberg, N. Bendsoe, J. Axelsson, S. Andersson-Engels, and S. Svanberg, "Photodynamic therapy: superficial and interstitial illumination," *J. Biomed. Opt.* **15**(4), 041502 (2010).
3. H.-P. Lassalle, D. Dumas, S. Gräfe, M.-A. D'Hallewin, F. Guillemin, and L. Bezdetnaya, "Correlation between in vivo pharmacokinetics, intratumoral distribution and photodynamic efficiency of liposomal mTHPC," *J. Controlled Release* **134**(2), 118–124 (2009).
4. A. Johansson, J. Svensson, N. Bendsoe, K. Svanberg, E. Alexandratou, M. Kyriazi, D. Yova, S. Gräfe, T. Trebst, and S. Andersson-Engels, "Fluorescence and absorption assessment of a lipid mTHPC formulation following topical application in a non-melanotic skin tumor model," *J. Biomed. Opt.* **12**(3), 034026 (2007).
5. J. R. Mourant, I. J. Bigio, D. A. Jack, T. M. Johnson, and H. D. Miller, "Measuring absorption coefficients in small volumes of highly scattering media: source-detector separations for which path lengths do not depend on scattering properties," *Appl. Opt.* **36**(22), 5655–5661 (1997).
6. J. R. Mourant, T. M. Johnson, G. Los, and I. J. Bigio, "Non-invasive measurement of chemotherapy drug concentrations in tissue: prelimi-

nary demonstrations of in vivo measurements," *Phys. Med. Biol.* **44**(5), 1397–1417 (1999).
7. L. Lilge, C. O'Carroll, and B. Wilson, "A solubilization technique for photosensitizer quantification in ex vivo tissue samples," *J. Photochem. Photobiol. B: Biol.* **39**(3), 229–235 (1997).
8. D. Jocham, H. Stepp, and R. Waidelich, "Photodynamic diagnosis in urology: state-of-the-art," *Eur. Urol.* **53**(6), 1138–1150 (2008).
9. Q. T. Nguyen, E. S. Olson, T. A. Aguilera, T. Jiang, M. Scadeng, L. G. Ellies, and R. Y. Tsien, "Surgery with molecular fluorescence imaging using activatable cell-penetrating peptides decreases residual cancer and improves survival," *Proc. Nat. Acad. Sci. USA* **107**(9), 4317–4322 (2010).
10. M. S. Eljamel, "Fluorescence image-guided surgery of brain tumors: Explained step-by-step," *Photodiagn. Photodyn. Ther.* **5**(4), 260–263 (2008).
11. N. Haj-Hosseini, J. Richter, S. Andersson-Engels, and K. Wårdell, "Optical touch pointer for fluorescence guided glioblastoma resection using 5-aminolevulinic acid," *Lasers Surg. Med.* **42**, 9–14 (2010).
12. A. Bogaards, H. Sterenborg, and B. Wilson, "In vivo quantification of fluorescent molecular markers in real-time: A review to evaluate the performance of five existing methods," *Photodiagn. Photodyn. Ther.* **4**(3), 170–178 (2007).
13. A. Bogaards, H. Sterenborg, J. Trachtenberg, B. Wilson, and L. Lilge, "In vivo quantification of fluorescent molecular markers in real-time by ratio imaging for diagnostic screening and image-guided surgery," *Lasers Surg. Med.* **39**(7), 605–613 (2007).
14. H. Stepp, T. Beck, W. Beyer, C. Pfaller, M. Schuppler, R. Sroka, and R. Baumgartner, "Measurement of fluorophore concentration in turbid media by a single optical fiber," *Med. Laser Appl.* **22**(1), 23–34 (2007).
15. M. M. Korol', A. S. Slesar', M. V. Parkhots, A. Y. Khairullina, and T. V. Ol'shanskaya, "Determination of photosensitizer concentration in biological tissues from diffuse reflectance and fluorescence," *J. Appl. Spectrosc.* **76**(2), 260–267 (2009).
16. C. T. Xu, N. Svensson, J. Axelsson, P. Svenmarker, G. Somesfalean, G. Chen, H. Liang, H. Liu, Z. Zhang, and S. Andersson-Engels, "Autofluorescence insensitive imaging using upconverting nanocrystals in scattering media," *Appl. Phys. Lett.* **93**(17), 171103 (2008).
17. V. Ntziachristos, J. Ripoll, L. V. Wang, and R. Weissleder, "Looking and listening to light: the evolution of whole-body photonic imaging," *Nat. Biotech.* **23**, 313–320 (2005).
18. V. Ntziachristos, "Fluorescence molecular imaging," *Annu. Rev. Biomed. Eng.* **8**(1), 1–33 (2006).
19. L. Sampath, W. Wang, and E. M. Sevick-Muraca, "Near infrared fluorescent optical imaging for nodal staging," *J. Biomed. Opt.* **13**(4), 041312 (2008).
20. C. T. Xu, J. Axelsson, and S. Andersson-Engels, "Fluorescence diffuse optical tomography using upconverting nanoparticles," *Appl. Phys. Lett.* **94**(25), 251107 (2009).
21. J. Svensson, A. Johansson, S. Gräfe, B. Gitter, T. Trebst, N. Bendsoe, S. Andersson-Engels, and K. Svanberg, "Tumor selectivity at short times following systemic administration of a liposomal temoporfin formulation in a murine tumor model," *Photochem. Photobiol.* **83**(5), 1211–1219 (2007).
22. G. Themelis, J. S. Yoo, K.-S. Soh, R. Schulz, and V. Ntziachristos, "Real-time intraoperative fluorescence imaging system using light-absorption correction," *J. Biomed. Opt.* **14**(6), 064012 (2009).
23. G. Alexandrakis, F. R. Rannou, and A. F. Chatziioannou, "Tomographic bioluminescence imaging by use of a combined optical-PET (OPET) system: a computer simulation feasibility study," *Phys. Med. Biol.* **50**(17), 4225–4241 (2005).
24. E. Alerstam, S. Andersson-Engels, and T. Svensson, "White Monte Carlo for time-resolved photon migration," *J. Biomed. Opt.* **13**(4), 041304 (2008).
25. H. J. van Staveren, C. J. M. Moes, J. van Marie, S. A. Prahl, and M. J. C. van Gemert, "Light scattering in Intralipid-10% in the wavelength range of 400-1100 nm," *Appl. Opt.* **30**, 4507–4514 (1991).
26. V. Engelhardt, B. Krammer, and K. Plaetzer, "Antibacterial photodynamic therapy using water-soluble formulations of hypericin or mTHPC is effective in inactivation of Staphylococcus aureus," *Photochem. Photobiol. Sci.* **9**(1), 365–369 (2010).

27. J. Buchholz, B. Kaser-Hotz, T. Khan, C. Rohrer Bley, K. Melzer, R. A. Schwendener, M. Roos, and H. Walt, "Optimizing photodynamic therapy: in vivo pharmacokinetics of liposomal meta-(tetrahydroxyphenyl)chlorin in feline squamous cell carcinoma," *Clin. Cancer Res.* **11**(20), 7538–7544 (2005).

28. R. L. P. van Veen, W. Verkruysse, and H. J. C. M. Sterenborg, "Diffuse-reflectance spectroscopy from 500 to 1060 nm by correction for inhomogeneously distributed absorbers," *Opt. Lett.* **27**(4), 246–248 (2002).

29. L. O. Svaasand, E. J. Fiskerstrand, G. Kopstad, L. T. Norvang, E. K. Svaasand, J. S. Nelson, and M. W. Berns, "Therapeutic response during pulsed laser treatment of port-wine stains: Dependence on vessel diameter and depth in dermis," *Lasers Med. Sci.* **10**, 235–243 (1995).

30. Z. Xu, J. Liu, and Y. L. Kim, "Diffuse light suppression of back-directional gating imaging in high anisotropic media," *J. Biomed. Opt.* **14**(3), 030510 (2009).

31. H. Xie, P. Svenmarker, S. Andersson-Engels, et al. "Pharmacokinetic and biodistribution study following systemic administration of Fospeg–a pegylated liposomal temoporfin formulation in a murine model," in preparation.

32. J. H. Lundeman, O. B. Jensen, P. E. Andersen, S. Andersson-Engels, B. Sumpf, G. Erbert, and P. M. Petersen, "High power 404 nm source based on second harmonic generation in PPKTP of a tapered external feedback diode laser," *Opt. Express* **16**(4), 2486–2493 (2008).

33. J. Swartling, A. Pifferi, A. M.K. Enejder, and S. Andersson-Engels, "Accelerated Monte Carlo models to simulate fluorescence spectra from layered tissues," *J. Opt. Soc. Am. A* **20**(4), 714–727 (2003).

34. E. Alerstam, S. Andersson-Engels, and T. Svensson, "Improved accuracy in time-resolved diffuse reflectance spectroscopy," *Opt. Express* **16**, 10440–10454 (2008).

35. B. Kruijt, S. Kascakova, H. S. de Bruijn, A. van der Ploeg-van den Heuvel, H. J. C. M. Sterenborg, and D. J. Robinson, "In vivo quantification of chromophore concentration using fluorescence differential path length spectroscopy," *J. Biomed. Opt.* **14**(3), 034022 (2009).

36. N. Bendsoe, L. Persson, A. Johansson, J. Axelsson, J. Svensson, S. Gräfe, S. Svanberg, and K. Svanberg, "Fluorescence monitoring of a topically applied liposomal temoporfin formulation and photodynamic therapy of nonpigmented skin malignancies," *J. Environ. Pathol. Toxicol. Oncol.* **26**(2), 117–126 (2007).